Optics Communications 352 (2015) 63–69

Contents lists available at ScienceDirect

Optics Communications

journal homepage: www.elsevier.com/locate/optcom

Study of spatial lateral resolution in off-axis digital holographic microscopy

Ana Doblas [a,*], Emilio Sánchez-Ortiga [a], Manuel Martínez-Corral [a], Jorge Garcia-Sucerquia [b,*]

[a] University of Valencia, 3D Imaging and Display Laboratory, Department of Optics, E-46100 Burjassot, Spain
[b] Universidad Nacional de Colombia Sede Medellin, School of Physics, A.A. 3840, Medellin 050034, Colombia

ARTICLE INFO

Article history:
Received 17 February 2015
Received in revised form
21 April 2015
Accepted 25 April 2015
Available online 30 April 2015

Keywords:
Digital holographic microscopy
Image formation
Digital processing

ABSTRACT

The lateral resolution in digital holographic microscopy (DHM) has been widely studied in terms of both recording and reconstruction parameters. Although it is understood that once the digital hologram is recorded the physical resolution is fixed according to the diffraction theory and the pixel density, still some researches link the resolution of the reconstructed wavefield with the recording distance as well as with the zero-padding technique. Aiming to help avoiding these misconceptions, in this paper we analyze the lateral resolution of DHM through the variation of those two parameters. To support our outcomes, we have designed numerical simulations and experimental verifications. Both the simulations and the experiments confirm that DHM is indeed resolution invariant in terms of the recording distance and the zero-padding provided that it operates within the angular spectrum regime.

1. Introduction

Digital holographic microscopy (DHM) is a well-established technique for MEMS evaluation [1–3], living cell screening [4–7] and particle tracking [8–13]. Based on the original Gabor's idea [14], DHM allows the retrieval of the complex wavefield scattered by samples from variety of fields [15–18]. The capacity of retrieving scattered complex wavefields powers DHM with the possibility of performing quantitative phase imaging (QPI). As in any microscopy technique, the lateral resolution has been a matter of great interest; since the onset of DHM many works have been published to master the spatial resolution of DHM and to find ways to improve it [4,19–24].

DHM is a hybrid imaging technique that can be understood as the application in cascade of two processes. The first stage is the optical recording of a digital hologram. In this stage the sampling frequency, the wavefield propagation, and interference phenomena determine which spatial frequencies are recorded. The second stage is the numerical recovery of the wavefield scattered by the object. The combined performance of these two stages, determines the spatial frequencies that compose the retrieved image, namely the spatial resolution of the technique. According to the classical definition in microscopy, the spatial resolution of a DHM is defined as the minimum distance between two point-objects such that they are distinguishable in the image retrieved from the hologram.

Although the conditions that allow DHM to operate in the diffraction limit regime [19] have already been established, many DHM systems do not operate in such regime and still remains some controversy about their resolution limit. Two parameters have been particularly studied: the recording distance [4,21,25] and the zero-padding of the digital hologram prior to the numerical reconstruction [21,26–29]. For the former it has been claimed [25] that out-of-focus holograms produce reconstructed images with better resolution than in-focus holograms. For the latter, zero-padding has been proposed as a method for controlling the resolution of reconstructed images [26,27].

In this paper, we assess the spatial resolution of DHM in terms of the recording distance and the zero-padding while the DHM operates in the angular spectrum domain [30], in off-axis architecture and at non-diffraction limit regime [19]. Our study confirms that DHM is indeed resolution invariant in terms of the recording distance and the zero-padding.

The paper is organized as follows: Section 2 reviews the basic theory that is behind the recording and reconstruction stages in an off-axis DHM. In Section 3, we define the resolution limit in DHM and present a model for the evaluation of the lateral resolution. The evaluation of the spatial lateral resolution as a function of the recording distance is presented in Section 4. In Section 5 the effects of the zero-padding on the spatial lateral resolution of the

* Corresponding authors.
E-mail addresses: a.isabel.doblas@uv.es (A. Doblas), jigarcia@unal.edu.co (J. Garcia-Sucerquia).

http://dx.doi.org/10.1016/j.optcom.2015.04.066
0030-4018/

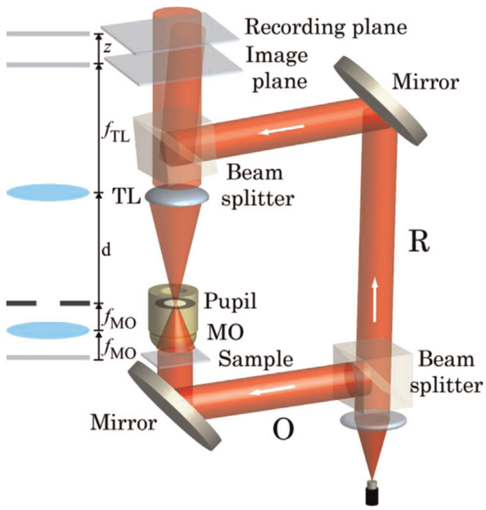

Fig. 1. Scheme of an off-axis DHM. In a general case, the MO and the TL are arranged in non-telecentric mode.

DHM are evaluated. The studies in Sections 4 and 5 are performed both numerically and experimentally. Finally, Section 6 is dedicated to summarize the main achievements of our research.

2. Fundamental of off-axis DHM

DHM is a hybrid imaging technique based on two stages: the optical recording of hologram and its numerical reconstruction. In the case of the off-axis architecture, the reconstruction stage can be performed after a single shot capture. As illustrated in Fig. 1, an optical microscope, known here as the host microscope, is inserted in one of the arms of a Mach–Zehnder interferometer. The light-beam emitted by a laser of wavelength λ_0 impinges on a beam splitter cube. One of the split beams illuminates the sample, $O(x, y)$, which is set at the front-focal-plane (FFP) of the microscope objective (MO). The image $O(x, y)$ is then obtained at the back-focal-plane (BFP) of the tube lens (TL). Commonly, this plane is named as the image plane (IP) of the optical microscope.

The complex wavefield $U_{IP}(x, y)$ produced by the microscope at the IP can be computed by application in cascade of ABCD transformations [31,32]. After regular algebra it is possible to obtain

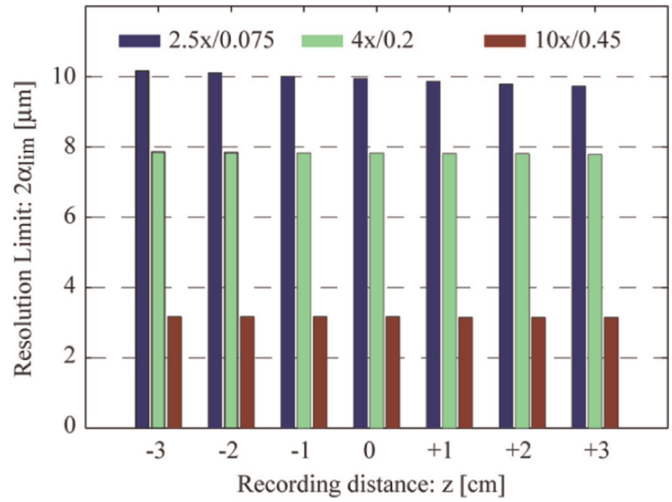

Fig. 3. Numerically-evaluated resolution limit vs. the recording distance for an off-axis DHM system.

$$U_{IP}(\boldsymbol{x}) = \frac{1}{M^2} e^{ik_0(2f_{MO}+d+f_{TL})} exp\left(i\frac{k_0}{2C}|\boldsymbol{x}|^2\right) \times \left\{O\left(\frac{\boldsymbol{x}}{M}\right) \otimes_2 \tilde{p}\left(\frac{\boldsymbol{x}}{\lambda_0 f_{TL}}\right)\right\}, \tag{1}$$

where $\boldsymbol{x} = (x, y)$ are the transverse coordinates, $k_0 = 2\pi/\lambda_0$ is the wave number, and $\tilde{p}(\boldsymbol{x})$ is the Fourier transform of the aperture transmittance of the imaging system. The lateral magnification, $M = -f_{TL}/f_{MO}$, does not depend on the distance, d, between the MO, the BFP and the TL.

The distance d, however, is a relevant parameter in performance of DHM, as shown recently [33,34]. In Eq. (1) we find a quadratic phase term whose radius of curvature

$$C = \frac{f_{TL}^2}{f_{TL} - d}, \tag{2}$$

appears due to the use of the microscope in non-telecentric regime ($d \neq f_{TL}$). As direct consequence of this phase term, the DHM becomes a shift-variant imaging system [22,33,34], with important ruining effects in the QPIs.

The irradiance pattern recorded on digital camera is the result of the interference between a tilted plane wave

$$R(\boldsymbol{x}) = \sqrt{I_R}\, exp(\mathbf{ik}\cdot\boldsymbol{x}), \tag{3}$$

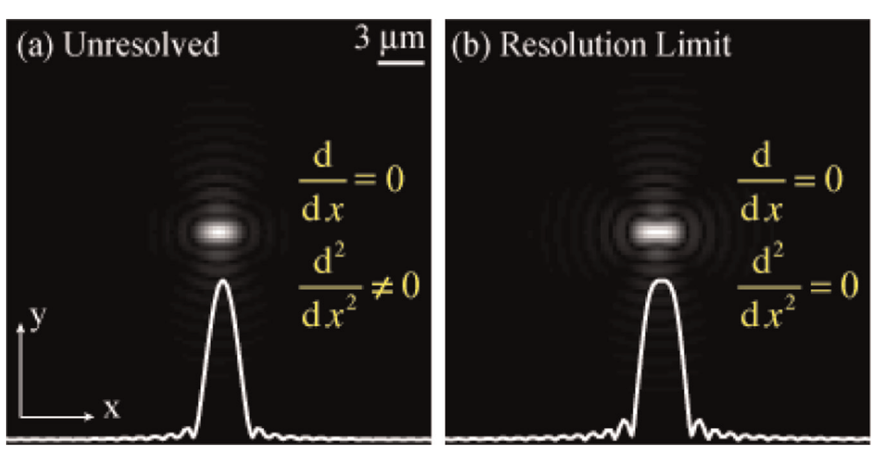

Fig. 2. Numerical test of the lateral spatial resolution. (a) Reconstructed image calculated from a simulated hologram of two points spaced $2\alpha = 0.6$ μm. (b) The same for two points separated $2\alpha_{lim} = 0.7$ μm. For the calculations we assumed a setup in which $\lambda_0 = 633$ nm, $M = -50$, $NA = 0.55$, $f_{TL} = 200$ mm, $d = 180$ mm, $z = +3$ cm and $N = 1024$ pixels.

with the U_{IP} (x) wavefield propagated by distance z from the IP

$$U(\boldsymbol{x}, z) = \frac{i}{\lambda_0 z} e^{ik_0 z} \left\{ U_{IP}(\boldsymbol{x}) \otimes_2 \ exp\left(i\frac{k_0}{2z} |\boldsymbol{x}|^2 \right) \right\}. \tag{4}$$

In Eq. (4), k=(k_x, k_y) is the wave vector of the plane wave and I_R its irradiance. Note that in Eq. (4) $z<0$ refers to planes located in front of the IP.

The irradiance pattern recorded by the sensor, called hologram, is given by

$$H(\boldsymbol{x}, z) = |U(\boldsymbol{x}, z)|^2 + |R(\boldsymbol{x})|^2 + U(\boldsymbol{x}, z)R^*(\boldsymbol{x}) + U^*(\boldsymbol{x}, z)R(\boldsymbol{x}), \tag{5}$$

where * is the complex-conjugate operator.

As clear from Eq. (5), the hologram is composed by four terms. The first two terms do not carry any information about the phase of the object and the angle of the reference wave. They produce, when Fourier transformed, the zero-order of diffraction (usually known as the DC term). The DC term is always placed at the center of the Fourier transform of the hologram. The third and fourth terms are identified as the $+1$ and -1 diffraction orders in the Fourier domain, respectively, and encode the whole sample information, both in amplitude and phase. Due to the off-axis configuration, the $+1$ and -1 diffraction orders are arranged symmetrically around the DC term in the Fourier space.

According to well-established reconstruction methods, the object information can be obtained by spatially filtering out the $+1$ term [35]. If the hologram, and therefore its Fourier transform, is composed by $N \times N$ pixels, the cropped $+1$ term is formed by $L \times L$ pixels. The value of L depends on different parameters [19], but always satisfying that $L < N/4$ when the hologram is correctly recorded. To calculate the reconstructed image, the $L \times L$ matrix is placed at the center of a new matrix which is $(N-L) \times (N-L)$ zero-padded. Then, by inverse Fourier transforming the new matrix, we obtain the spatial filtered $U(\boldsymbol{x}, z)$. To reconstruct the image at the IP, $U_{IP}(\boldsymbol{x})$, it is necessary the application of well-known back-propagation algorithms [15–18].

3. Spatial lateral resolution in off-axis DHM

The spatial resolution limit in off-axis DHM must be defined as in any conventional imaging technique; namely the minimum distance between two object points of equal irradiance that produce two distinct reconstructed images. Since DHM is a hybrid technique, the achievable spatial resolution does not depend only on diffraction effects. To preserve the resolution imposed by the host microscope, the DHM recording should be performed in such a way that there is no overlapping between the DC term and the ±1 diffraction orders. In such case it is possible to filter out the $+1$ order without losing spatial frequencies and without producing artifacts proceeding from the DC term [19].

To evaluate the resolution of a DHM, we consider an object composed by two coherent point-sources separated by a distance 2α and placed symmetrically to the optical axis at the object plane. Assuming in such case that

$$O(\boldsymbol{x}) = \sqrt{I_0}\,[\delta(x-\alpha, y) + \delta(x+\alpha, y)], \tag{6}$$

where I_0 is the source irradiance, we can rewrite Eq. (4) as

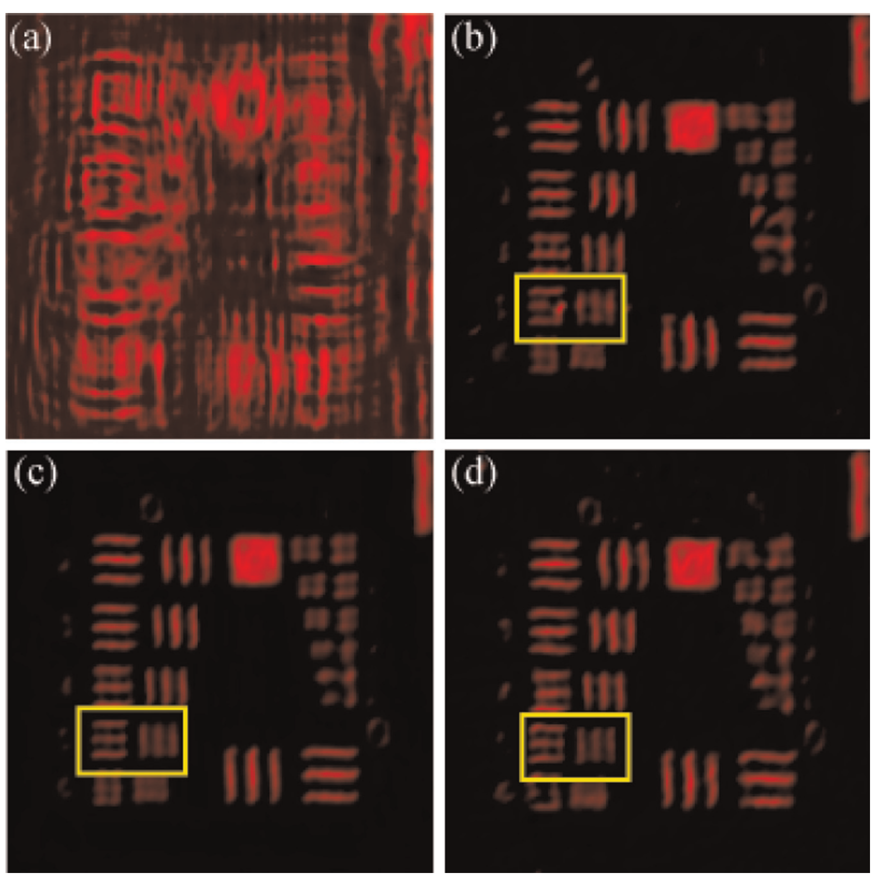

Fig. 4. Simulated images of an USAF chart: (a) modeled hologram recorded at $z=-3$ cm. (b)–(d) Reconstructed image for a hologram recorded: (b) $z=-3$ cm, (c) $z=0$ cm (IP), and (d) $z=+3$ cm. Yellow rectangles highlight the smallest resolvable element. The image area is 331×331 μm^2. (For interpretation of the references to color in this figure legend, the reader is referred to the web version of this article.)

$$U(\boldsymbol{x}, z) = 4\lambda_0^2 f_{TL}^2 M\sqrt{I_0}\, e^{i\frac{2\pi}{\lambda_0}(2f_{MO}+d+f_{TL}+z)} \times exp\left(i\frac{\pi}{\lambda_0 z}|\boldsymbol{x}|^2\right) \times \left\{exp\left(-i\frac{\pi}{\lambda_0 z}\frac{C}{C+z}|\boldsymbol{x}|^2\right)\otimes_2\left[\cos\left(\frac{2\pi}{\lambda_0}\frac{M\alpha}{z}x\right) p\left(-\frac{f_{TL}}{z}\boldsymbol{x}\right)\right]\right\}. \tag{7}$$

The interference of this amplitude distribution with a reference plane wave $R(\boldsymbol{x})$ of the type of Eq. (3) produces the corresponding hologram $H(\boldsymbol{x}, z)$ as given by Eq. (5). The modeled hologram is then reconstructed to evaluate the achieved spatial resolution by means of Sparrow's criterion [36]. According to the modified Sparrow criterion [37], the resolution limit is defined as the distance, $2\alpha_{\text{lim}}$, between two point-objects. This distance is obtained when the second derivative of the intensity curve distribution vanishes at the midpoint between the two images. Additionally, at this midpoint the first derivative of the intensity curve should become also zero. Note that the latter statement considers the possibility that the two points do not have the same intensity. As illustrated in Fig. 2, panels (a) and (b) show an unresolved/resolved couple of point-objects. For (a)/(b) the first and second derivatives were evaluated to follow Sparrow's metric.

In this work, the spatial lateral resolution in off-axis DHM is then evaluated, both numerically and experimentally, as the recording distance and the zero-padding are changed. Numerically, different holograms are modeled following Eq. (7) and the above-described Sparrow method applied. Experimentally, holograms of an USAF test target 1951 are recorded and reconstructed; direct inspection of the reconstructed images allows directly the evaluation of the spatial lateral resolution performance in off-axis DHM.

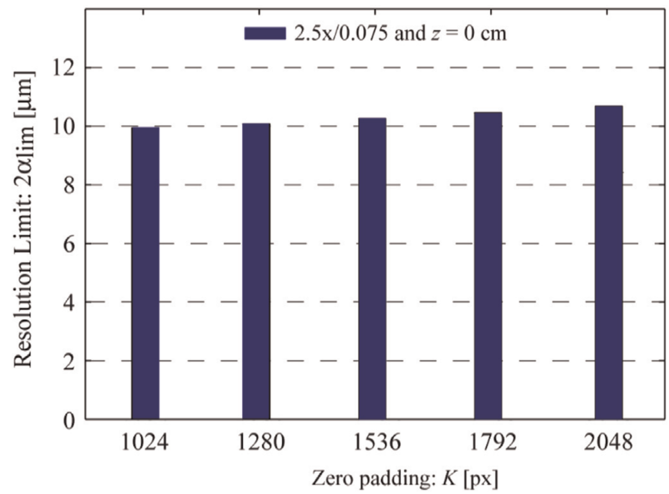

Fig. 6. Numerically-evaluated resolution limit vs. the different number of pixels during the zero-padding operation for a hologram recorded at the IP.

4. Spatial lateral resolution vs. recording distance

The recording distance is one of the parameters set to vary the spatial lateral resolution of off-axis-DHM [4,21,25]. In this section we evaluate, both numerically and experimentally, how the recording distance z of the digital hologram, varied within the angular spectrum regime, can modify the spatial lateral resolution.

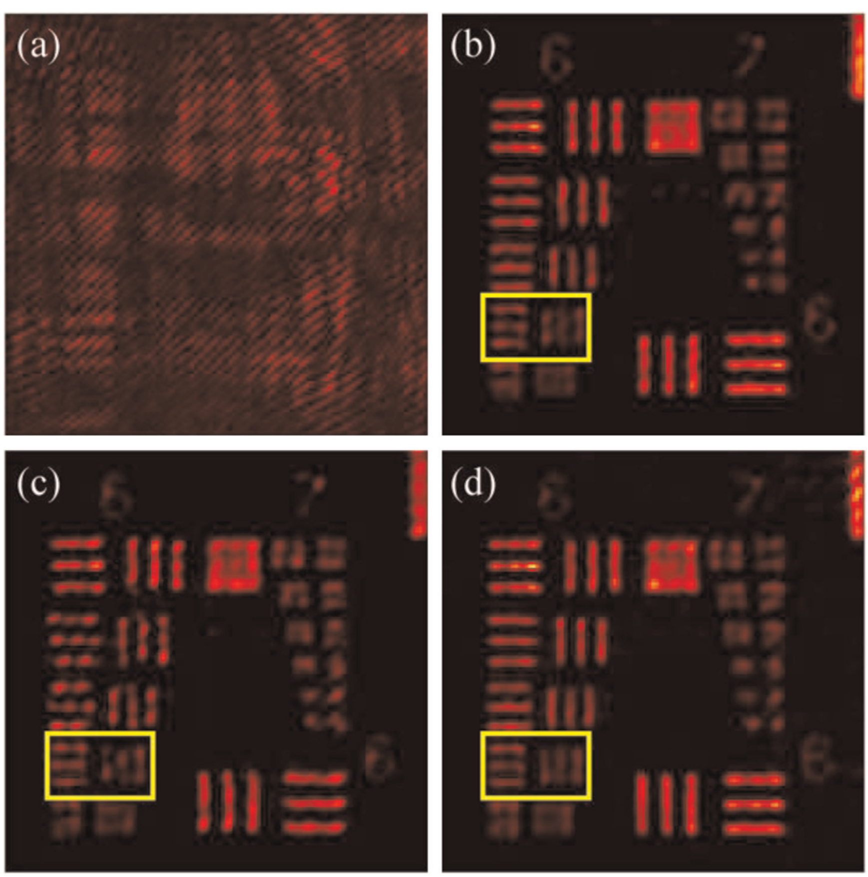

Fig. 5. Experimental images of a typical resolution test: (a) hologram recorded at $z = -3$ cm. (b)–(d) Reconstructed images for DHM: (b) $z = -3$ cm, (c) $z = 0$ cm (IP), and (d) $z = +3$ cm. The yellow rectangles highlight the smallest resolvable group. The image area is 331×331 μm^2. (For interpretation of the references to color in this figure legend, the reader is referred to the web version of this article.)

4.1. Numerical modeling

To face the numerical analysis we proceed as follows. First, we set as input value for the separation between the two point sources $2\alpha = 0.47\lambda_0/NA$ [38], namely, the theoretical Sparrow resolution limit. Second, we compute the numerical hologram for a given distance z. Third, we calculate the Fourier transform of the hologram and crop the term to filter out the $+1$ diffracted order. Then, the filtered $+1$ term is zero-padded around up to compose a new matrix of $N \times N$ pixels. Finally, by performing the inverse Fourier transform and applying a refocusing algorithm we obtained the reconstructed image.

To apply the Sparrow criterion we build a 1D function with the irradiance values in the line connecting the reconstructed point sources, see Fig. 2. As this profile is composed by discrete values, we use an interpolation method to create a continuous distribution. Aiming to preserve the shape of the data, we use the piecewise cubic Hermite interpolation (PCHIP) provided by Curve Fitting Toolbox in Matlab©. Then we evaluate the first and second derivatives at the midway point between the reconstructed points. If the values of these derivatives are different from zero (Fig. 2(a)), then we increase 2α in steps of 0.01 μm. The iterative process ends when the first and second derivatives vanish, see Fig. 2(b).

Following this procedure we perform numerical experiments considering three different MOs: (i) $2.5\times/0.075$, (ii) $4\times/0.2$ and (iii) $10\times/0.45$. For the three systems we have chosen the same TL, $f_{TL} = 200$ mm. The modeled digital holograms are calculated assuming $\lambda_0 = 633$ nm and a CCD composed by of $N \times N = 1024 \times 1024$ square pixels of 6.9 μm in side. In our calculations, we have also assumed a non-telecentric arrangement with offset, $f_{TL} - d = 20$ mm.

The spatial lateral resolution was then calculated for holograms recorded at: $z = -3, -2, -1, 0, +1, +2, +3$ cm from the IP. Fig. 3 shows the computed values of the resolution limit for the three imaging systems. We find that the resolution limit is affected very slightly; while this variation is less than 2% for the $2.5\times$ MO, it is less than 0.6% for the other MOs. Because the largest, indeed very small, variation of the spatial lateral resolution as the recording distance varies is observed for the $2.5\times$ MO, the further analysis is carried out with this imaging system.

To compare the numerically-evaluated and the experimental results we have also performed a numerical experiment using the USAF chart as the object. In this simulation, the imaging system was composed by the $2.5\times$ MO and the TL of $f_{TL} = 200$ mm. Fig. 4 depicts a modeled hologram and the reconstructed images obtained for different recording distances, z. In panel (a) we show the modeled out-of-focus hologram for a recording distance of $z = -3$ cm. In panels from (b) to (d) are the reconstructed images for $z = -3$ cm, $z = 0$ cm (IP), and $z = +3$ cm, in that order. The yellow rectangles highlight the smallest resolved element for each image. Clearly, no variation of the resolution limit in terms of the recording distance is observed. These results mean that the very small variation on the spatial resolution as the recording distance varies, as observed in Fig. 3 for two point sources, is not observable as a real object is imaged. The experimental results of the following section will help us to clarify this point.

4.2. Experimental evaluation

Using a setup equivalent to the one sketched in Fig. 1 we have recorded the experimental hologram of an USAF resolution chart illuminated with a monochromatic plane wave produced from a

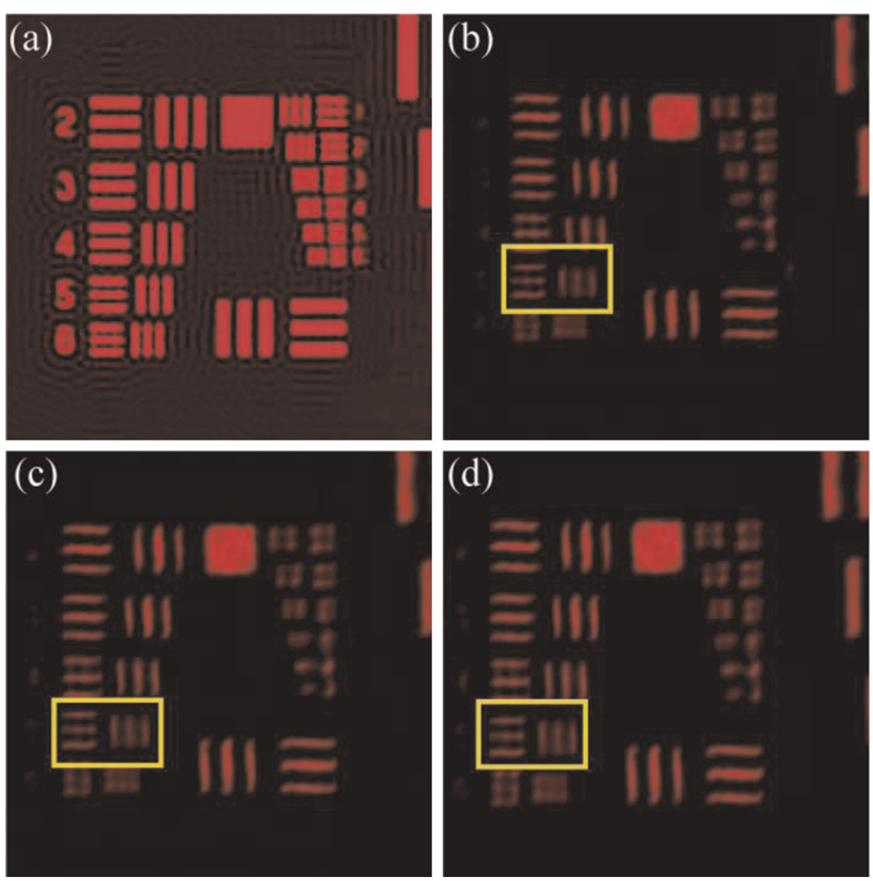

Fig. 7. Simulated images of an USAF chart: (a) in-focus hologram. (b)–(d) Reconstructed absolute amplitude for a DHM applying zero padding: (b) $K = N = 1024$, (c) $K = 1536$ and (d) $K = 2048$. Smallest resolvable group is marked by a yellow rectangle. (For interpretation of the references to color in this figure legend, the reader is referred to the web version of this article.)

He–Ne laser (λ=633 nm). Again, the DHM was built with a 2.5 ×/0.075 MO and a TL of f_{TL}=200 mm. Besides, the DHM system also operated at non-telecentric regime with an offset of $f_{TL}-d$=20 mm. Experimental holograms were acquired on a CCD sensor with 1024 × 1024 square pixels of 6.9 μm in side. To adjust the object and the reference intensities a neutral-density filter was inserted at the reference arm.

Seven experimental holograms were recorded at equally-space distances around the IP, from $z=-3$ cm to $z=+3$ cm. Particularly, the experimental out-of-focus hologram recorded at $z=-3$ cm from the IP is shown in Fig. 5(a). After applying the reconstruction process, we obtained the reconstructed images in Fig. 5(b)–(d). From these panels one can see that the spatial lateral resolution does not vary as the recording distance is changed. The yellow squares, which highlight the smallest resolved details, are placed over the same elements of the resolution target, see panels from (b) to (d). These experimental results coincide with those modeled in the previous section and illustrated in Fig. 4.

Both, the numerical and experimental results, show no variation of the achieved spatial resolution in off-axis DHM as the recording distance changes. These results allow the stating that off-axis DHM is a resolution-invariant imaging system as the recording distance varies.

5. Spatial lateral resolution vs. zero-padding

As stated above, the zero-padding technique has been proposed as a method to control the resolution limit in DHM [21,26–29]. In the sense of modifying the spatial resolution via the zero-padding, the latter is understood as the use of a new matrix of $K \times K$ pixels, being $K \geq N$, to perform the spatial filter of the +1 term. In this section, we examine the dependence of the resolution limit on the zero-padding technique. Similarly to Section 4, this evaluation is performed both numerically and experimentally. Because in the above section we have found that the largest variation on the spatial resolution is observed when a 2.5 × MO is used, in this study on the zero-padding we use the same objective. Additionally, once the invariance of the spatial lateral resolution with the recording distance has been shown, the study in this section is limited, without lack of generality, to holograms recorded at the IP.

5.1. Numerical modeling

Performing the same numerical procedure described in Section 4, now the Sparrow's resolution limit of a DHM is studied as a function of the size of the new matrix, $K \times K$. Particularly, the lateral resolution is calculated for five different sizes of the new matrix: K=1024 (K=N), 1280, 1536, 1792 and 2048 pixels.

The modeled results are illustrated in Fig. 6. Numerically we observe that the spatial lateral resolution is very slightly increased, less than 3%, by increasing the number of pixels of the new matrix for performing the spatial filter. As a consequence of this result, we have then the need of investigating if that order of variation can be observed in an imaging system when imaging a real object rather than ideal point-sources. To attempt this evaluation we have numerically modeled the imaging of a USAF 1951 test chart in our off-axis DHM. Using the modeled in-focus hologram (see Fig. 7(a)), we have varied the size of the new matrix K from K=N=1024 pixels to K=2048 pixels. The modeled reconstructed images are

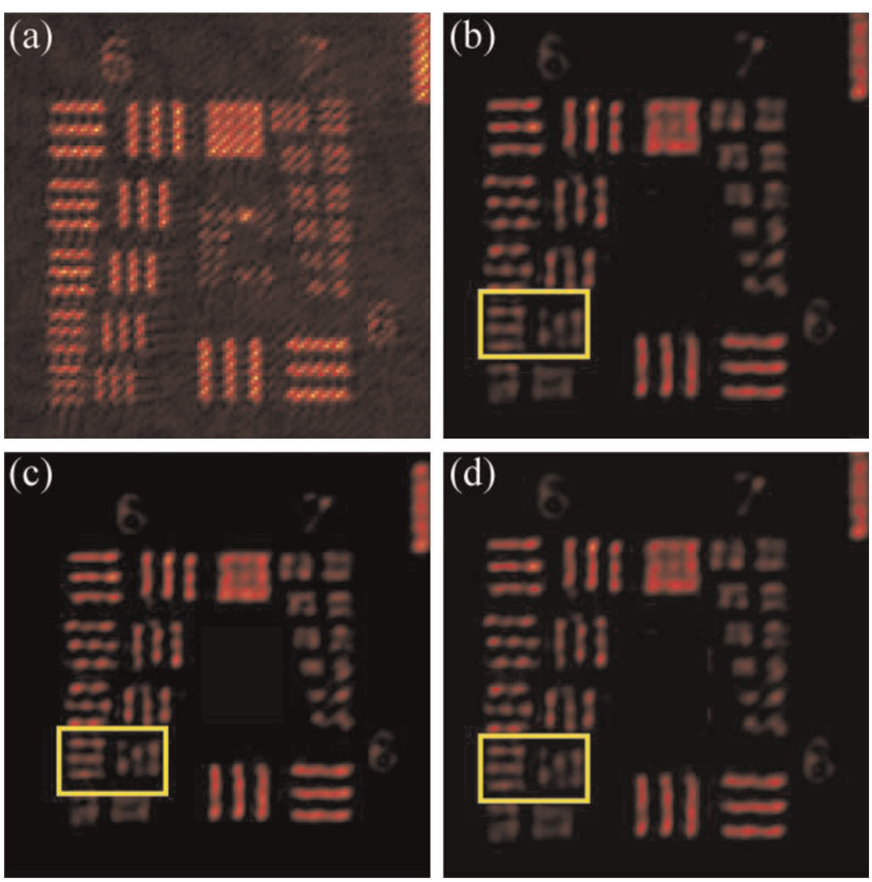

Fig. 8. Groups 6 and 7 of a negative 1951 USAF resolution chart: (a) experimental hologram recorded at the IP. (b)–(d) Reconstructed absolute amplitude images for DHM applying zero padding: (b) K=N=1024, (c) K=1536 and (d) K=2048. Smallest resolvable group is marked by a yellow rectangle. (For interpretation of the references to color in this figure, the reader is referred to the web version of this article.)

shown from Fig. 7(b) to (d). The smallest resolved element of each panel is marked by a yellow rectangle. From this figure, it is clear that no change of the resolution limit has been detected by varying the zero-padding size as a real object is imaged.

5.2. Experimental evaluation

To study experimentally the resolution limit as a function of different sizes of the zero-padding operation, we used the experimental in-focus hologram shown in Fig. 8(a). Panels from (b) to (d) in Fig. 8 illustrate the reconstructed images as the value of K ranges from 1024 pixels to 2048 pixels. Again, yellow rectangles highlight the smallest resolvable elements. Evidently, the experimental resolution limit of the DHM is not modified by increasing K.

From the numerical and experimental results obtained in this section, we can conclude that the lateral resolution in off-axis DHM is not modified by the zero-padding operation. This result is compatible with the ones reported by Picart et al. [21]. Therefore, off-axis DHM can be also claimed as resolution-invariant imaging system in terms of the zero-padding operation.

6. Conclusions

The lateral resolution in off-axis DHM has been discussed in terms of the recording distance and the zero-padding technique in the angular spectrum regime. We have numerically and experimentally verified that neither the recording distance nor the zero-padding modify the spatial resolution of DHM. For an off-axis DHM operating in the angular spectrum and the non-diffraction limit regime, the changes in the recording distance are not large enough to introduce merging of the ± 1 diffraction orders with the zero-order which definitely would alter the spatial resolution of the DHM. For the same regime of operation, we have shown that zero-padding does not control the resolution capability of the off-axis DHM. Using zero-padding operation, the resolution remains unaffected. This operation only changes the effective pixel size, namely a magnification operation is performed with the zero-padding. The findings reported here contribute to consolidate the DHM as a microscopy technique with no variance on its spatial resolution as regard with the operation parameters and the user expertise.

Acknowledgments

This research was supported in part from the Ministerio de Economia y Competitividad, Spain, under Grant DPI2012-32994, and also from Generalitat Valenciana under Grant PROMETEOII/2014/072. J. Garcia-Sucerquia acknowledges the support from Universidad Nacional de Colombia, Hermes Grant 19384 and the Programa de Internacionalización del Conocimiento. A. Doblas welcomes funding from the University of Valencia through the predoctoral fellowship program “Atracció de Talent” and from Universidad Nacional de Colombia Sede Medellín.

References

[1] G. Coppola, S. De Nicola, P. Ferraro, A. Finizio, S. Grilli, M. Iodice, C. Magro, G. Pierattini, Characterization of MEMS structures by microscopic digital holography, Proc. SPIE 4945 (2003) 71.
[2] A. Asundi, Digital Holography for MEMS and Microsystem Metrology, Wiley, Chichester, 2011.
[3] Y. Emery, E. Solanas, N. Aspert, A. Michalska, J. Parent, E. Cuche, MEMS and MOEMS resonant frequencies analysis by digital holography microscopy (DHM), Proc. SPIE 8614 (2013) 86140A.
[4] B. Kemper, D. Carl, J. Schnekenburger, I. Bredebusch, M. Schäfer, W. Domschke, G. von Bally, Investigation on living pancreas tumor cells by digital holographic microscopy, J. Biomed. Opt. 11 (2006) 34005.
[5] B. Kemper, A. Bauwens, A. Vollmer, S. Ketelhut, P. Langehanenberg, J. Müthing, H. Karch, G. von Bally, Label-free quantitative cell division monitoring of endothelial cells by digital holographic microscopy, J. Biomed. Opt. 15 (2010) 036009–036015.
[6] N. Pavillon, J. Kühn, C. Moratal, P. Jourdain, C. Depeursinge, P.J. Magistretti, P. Marquet, Early cell death detection with digital holographic microscopy, PLoS One 7 (2012) e30912.
[7] M. Puthia, P. Storm, A. Nadeem, S. Hsiung, C. Svanborg, Prevention and treatment of colon cancer by peroral administration of HAMLET (human α-lactalbumin made lethal to tumour cells), Gut 63 (2014) 131–142.
[8] C.J. Mann, L. Yu, M.K. Kim, Movies of cellular and sub-cellular motion by digital holographic microscopy, Biomed. Eng. Online 5 (2006) 21.
[9] K. Jeong, L. Peng, J.J. Turek, M.R. Melloch, D.D. Nolte, Fourier-domain holographic optical coherence imaging of tumor spheroids and mouse eye, Appl. Opt. 44 (2005) 1798–1805.
[10] J. Kühn, F. Montfort, T. Colomb, B. Rappaz, C. Moratal, N. Pavillon, P. Marquet, C. Depeursinge, Submicrometer tomography of cells by multiple-wavelength digital holographic microscopy in reflection, Opt. Lett. 34 (2009) 653–655.
[11] N. Warnasooriya, F. Joud, P. Bun, G. Tessier, M. Coppey-Moisan, P. Desbiolles, M. Atlan, M. Abboud, M. Gross, Imaging gold nanoparticles in living cell environments using heterodyne digital holographic microscopy, Opt. Express 18 (2010) 3264–3273.
[12] J. Kühn, E. Shaffer, J. Mena, B. Breton, J. Parent, B. Rappaz, M. Chambon, Y. Emery, P. Magistretti, C. Depeursinge, P. Marquet, G. Turcatti, Label-free cytotoxicity screening assay by digital holographic microscopy, Assay Drug Dev. Technol. 11 (2013) 101–107.
[13] H. Sun, B. Song, H. Dong, B. Reid, M.A. Player, J. Watson, M. Zhao, Visualization of fast-moving cells in vivo using digital holographic video microscopy, J. Biomed. Opt. 13 (2013) 014007–014009.
[14] D. Gabor, A new microscopic principle, Nature 161 (1948) 777.
[15] T. Kreis, Handbook of Holographic Interferometry, Wiley, Chichester, 2004.
[16] M.K. Kim, Principles and techniques of digital holographic microscopy, SPIE Rev. 1 (2010) 018005.
[17] G. Popescu, Quantitative Phase Imaging of Cells and Tissues, McGraw-Hill, New York, 2011.
[18] P. Picart, J.-C. Li, Digital Holography, Wiley, Chichester, 2012.
[19] E. Sánchez-Ortiga, A. Doblas, G. Saavedra, M. Martínez-Corral, J. Garcia-Sucerquia, Off-axis digital holographic microscopy: practical design parameters for operating at diffraction limit, Appl. Opt. 53 (2014) 2058–2066.
[20] L. Xu, X. Peng, Z. Guo, J. Miao, A. Asundi, Imaging analysis of digital holography, Opt. Express 13 (2005) 2444–2452.
[21] P. Picart, J. Leval, General theoretical formulation of image formation in digital Fresnel holography, J. Opt. Soc. Am. A 25 (2008) 1744–1761.
[22] D.P. Kelly, B.M. Hennelly, N. Pandey, T.J. Naughton, W.T. Rhodes, Resolution limits in practical digital holographic systems, Opt. Eng. 48 (2009) 095801–095813.
[23] D. Claus, D. Iliescu, P. Bryanston-Cross, Quantitative space-bandwidth product analysis in digital holography, Appl. Opt. 50 (2011) H116–H127.
[24] Y. Hao, A. Asundi, Resolution analysis of a digital holography system, Appl. Opt. 50 (2011) 183–193.
[25] D. Claus, D. Iliescu, Optical parameters and space-bandwidth product optimization in digital holographic microscopy, Appl. Opt. 52 (2013) A410–A422.
[26] L. Yu, M.K. Kim, Pixel resolution control in numerical reconstruction of digital holography Lingfeng, Opt. Lett. 31 (2006) 897–899.
[27] S. De Nicola, P. Ferraro, S. Grilli, L. Miccio, R. Meucci, P.K. Buah-Bassuah, F. T. Arecchi, Infrared digital reflective-holographic 3D shape measurements, Opt. Commun. 281 (2008) 1445–1449.
[28] N. Verrier, M. Atlan, Off-axis digital hologram reconstruction: some practical considerations, Appl. Opt. 50 (2011) H136–H146.
[29] N. Muhammad, D.-G. Kim, A simple approach for large size digital off-axis hologram reconstruction-tags: digital image processing image reconstruction, in: Proceedings of the World Congress on Engineering (WCE), Vol. II, 2012, 6.
[30] D. Mendlovic, Z. Zalevsky, N. Konforti, Computation considerations and fast algorithms for calculating the diffraction integral, J. Mod. Opt. 44 (1997) 407–414.
[31] S.A. Collins, Lens-system diffraction integral written in terms of matrix optics, J. Opt. Soc. Am. 60 (1970) 1168–1177.
[32] D.S. Goodman, General principles of geometrical optics, in: M. Bass (Ed.), Handbook of Optics, McGraw-Hill, New York, 1995.
[33] A. Doblas, E. Sánchez-Ortiga, M. Martínez-Corral, G. Saavedra, P. Andrés, J. Garcia-Sucerquia, Shift-variant digital holographic microscopy: inaccuracies in quantitative phase imaging, Opt. Lett. 38 (2013) 1352–1354.
[34] A. Doblas, E. Sánchez-Ortiga, M. Martínez-Corral, G. Saavedra, J. Garcia-Sucerquia, Accurate single-shot quantitative phase imaging of biological specimens with telecentric digital holographic microscopy, J. Biomed. Opt. 19 (2014) 46022–46028.
[35] E. Cuche, P. Marquet, C. Depeursinge, Spatial filtering for zero-order and twin-image elimination in digital off-axis holography, Appl. Opt. 39 (2000) 4070–4075.
[36] M. Born, E. Wolf, Principles of Optics, Cambridge University Press, Cambridge, 1999.
[37] T. Asakura, Resolution of two unequally bright points with partially coherent points, Nouv. Rev. Opt. 5 (1974) 169–177.
[38] A. Lipson, S.G. Lipson, H. Lipson, Optical Physics, Cambridge University Press, Cambrigde, 2010.